THE ASTROPHYSICAL JOURNAL, 435:22–36, 1994 November 1

PAST AND FUTURE STAR FORMATION IN DISK GALAXIES

ROBERT C. KENNICUTT, JR., AND PETER TAMBLYN
Steward Observatory, University of Arizona, Tucson, AZ 85721

AND

CHARLES W. CONGDON
1943 SE 113th Ave, Portland, OR 97216
Received 1994 February 17; accepted 1994 May 5

ABSTRACT

We have combined Hα and *UBV* measurements of 210 nearby Sa–Irr galaxies with new photometric synthesis models to reanalyze the past and future star formation timescales in disks. The integrated photoionization rates and colors of disks are best fitted by a stellar initial mass function (IMF) which is enriched in massive stars by a factor of 2–3 relative to the Scalo solar neighborhood IMF. We have used published surface photometry of spiral galaxies to analyze the star formation histories of disks independent of their bulge properties. The ratio of the current star formation rate (SFR) to the average past rate increases from of order 0.01 in Sa galaxies to 1 in Sc–Irr disks. This confirms that the pronounced change in the photometric properties of spiral galaxies along the Hubble sequence is predominantly due to changes in the star formation histories of *disks*, and only secondarily to changes in the bulge/disk ratio. A comparison of current SFRs and gas masses of the sample yields median timescales for gas consumption of ~3 Gyr, in the absence of stellar recycling. However, a proper time-dependent treatment of the gas return from stars shows that recycling extends the gas lifetimes of disks by factors of 1.5–4 for typical disk parameters. Consequently the current SFRs in many (but not all) disks can be sustained for periods comparable to the Hubble time.

Subject headings: galaxies: evolution — galaxies: luminosity function, mass function — galaxies: spiral — galaxies: stellar content — stars: formation

1. INTRODUCTION

One of the important outstanding problems in extragalactic astronomy is determining the star formation history of the universe, and its variation with galaxy type and environment. The development of empirical methods for measuring star formation rates (SFRs) in galaxies allows us to study the stellar birthrate histories of these galaxies and compare the results with observations of distant galaxies at cosmological lookback times. The SFR data can also be combined with H I and CO measurements to extrapolate the future timescales for star formation in galaxies.

Most previous systematic studies of SFRs in disk and irregular galaxies are consistent with a common picture, in which the variation of the UV-visible colors and Hα emission properties of galaxies along the Hubble sequence can be attributed to underlying variations in their stellar birthrate histories (Kennicutt 1983, 1986, Gallagher, Hunter, & Tutukov 1984; Isserstedt & Schindler 1986; Sandage 1986). These results confirm and quantify the general picture revealed by modeling of the broadband colors of galaxies (Roberts 1963; Searle, Sargent, & Bagnuolo 1973; Larson & Tinsley 1978). In this picture early-type galaxies (types S0–Sb) represent systems which formed most of their gas into stars on timescales much less than the Hubble time, while the disks of late-type systems (Sc–Im) have formed stars at roughly a constant rate since they formed. The same analyses yield future star formation timescale for the latter galaxies of ~4–7 Gyr (Larson, Tinsley, & Caldwell 1980; Kennicutt 1983; Donas et al. 1987).

Although the qualitative foundation of the evolutionary picture appears to be firmly established, several important questions remain. For example, most analyses of the evolutionary properties of spirals are based on integrated photometric measurements, which include both the star forming disks and the older spheroids. At least part of the trend toward older populations in early-type spirals is due to nothing more than the increased bulge/disk fractions in these systems, and some workers have suggested that the evolutionary properties of *disks* are nearly independent of morphological type (e.g., Devereux & Young 1991). It is important to resolve this question by comparing the star formation properties of disks independently of their spheroid properties. Another major question is the role of variations in the stellar initial mass function (IMF). The derived SFRs and stellar birthrate histories are sensitive to the form and variation (if any) in the IMF, so much so that most of the variation in photometric properties of galaxies could be reproduced by invoking extreme variations in the IMF (Larson 1986). Although current observations make it very difficult to rule out systematic IMF variations, one can at least test whether the photometric properties of the disks of external galaxies are consistent with IMFs derived locally.

Perhaps the most puzzling result from the earlier studies is the relatively short inferred timescale for gas consumption. Roberts (1963) made the first comprehensive study of gas depletion times for disks and derived a mean time which was longer than the Hubble time. Subsequent studies, however, have yielded mean "Roberts times" of only a few Gyr, suggesting that we may live in an epoch in which late-type spirals are being transformed into early-type systems, or alternatively that large amounts of infall may be needed to sustain the star formation in late-type disks (e.g., Pfenniger, Combes, & Martinet 1993). This paradox has never been completely resolved.

Several recent observations and theoretical advances motivate a reexamination of the stellar birthrate histories of disks. Spatially resolved stellar surface photometry, H I, and CO

observations are now available for large numbers of galaxies, sufficient to study the evolutionary properties of disks over a wide range of Hubble type. On the theoretical side, improved stellar evolution and atmosphere models make it possible to apply updated photometric synthesis models to the problem, and to construct realistic time-dependent models for the gas consumption, star formation and recycling in disks. Although the importance of the latter has been emphasized in the context of Galactic chemical evolution (Truran & Cameron 1971; Ostriker & Thuan 1975), the star formation properties of external galaxies have usually been interpreted using an instantaneous recycling approximation.

This paper presents an updated analysis of the past and future star formation timescales in galaxies. The objectives are to update and extended a previous study of this problem (Kennicutt 1983; hereafter denoted K83), and to address the questions outlined above. The paper is organized as follows: In § 2 we describe the data set used for this analysis and in § 3 we describe the updated photometric synthesis models which we have computed for this study. The main results of the paper are presented in § 4–6. In § 4 we use the observed *UBVR* and Hα properties of spiral and irregular galaxies to constrain the IMF and compare the range of IMFs with those measured in the solar neighborhood and in luminous starburst galaxies. In § 5 we derive the star formation histories of disks for different galaxy types and compare the results with previous studies. In § 6 we derive the distribution of gas consumption and future star formation timescales, under the usual instantaneous recycling approximation. An updated time-dependent recycling model is presented and is used to demonstrate the importance of stellar mass return in extending the star formation lifetimes of galaxies. A brief summary and comparison with previous work is presented in § 7.

2. DATA

Following K83 we adopt as our primary star formation tracers the integrated Hα emission-line luminosities and equivalent widths of galaxies. The Hα luminosity provides a direct measure of the global photoionization rate, which can be used in turn to reliably estimate the SFR in massive ($> 10\ M_\odot$) stars. Extrapolation to a total SFR, integrated over all stellar masses, in accomplished either by adopting a priori a given IMF, or by using the observed Hα equivalent widths and broad-band colors of galaxies to constrain the IMF, as described in § 3. SFRs derived from this method are in good agreement with those derived from other tracers such as ultraviolet continuum luminosities (Buat 1992) or direct measurements of the OB stellar populations (Vacca 1994).

Our primary databases are the Hα + [N II] surveys of Kennicutt & Kent (1983) and Romanishin (1990). Both data sets consist of large-aperture photoelectric measurements of integrated fluxes, measured through filters which include the Hα and [N II] λλ6548, 6583 emission lines, and two continuum sidebands. Following K83 we will use the combined Hα and [N II] fluxes and apply a mean correction factor for the [N II] contamination. Throughout this paper we adopt [N II]/Hα = 0.5, the mean value derived from integrated spectra of galaxies by Kennicutt (1992).

The sample includes galaxies with morphological types in the range Sa–Sm, as classified in Sandage & Tammann (1981; RSA), de Vaucouleurs, de Vaucouleurs, & Corwin (1976; RC2), or de Vaucouleurs et al. (1991; RC3). We excluded peculiar objects, including interacting starburst galaxies, those with luminous Seyfert or low-ionization nuclear emission-line region (LINER) nuclei, and those selected by Romanishin (1990) as having extreme low surface brightness disks. The main purpose of this selection was to guarantee a sample of normal disk galaxies, against which other class of objects (e.g., interacting galaxies, low surface brightness galaxies) can be compared. Systems with luminous active galactic nuclei (AGNs) were excluded to avoid possible problems with nonstellar Hα + [N II] emission. A total of 135 galaxies in Kennicutt & Kent (1983) and 69 in Romanishin (1990) met these selection criteria. In order to increase the coverage of the sample, especially for early-type galaxies with weak Hα emission we added to the data set CCD measurements of eight S0/a–Sa galaxies from Caldwell et al. (1991), CCD measurements of 45 galaxies from Kennicutt & Martin (1994), and integrated spectra of 32 spiral and irregular galaxies from Kennicutt (1992). Global Hα measurements of M31 were taken from Walterbos & Braun (1994).

The entire sample contains 210 galaxies, including 50 objects measured in at least two independent surveys. This overlap allows us to compare the photometric scales between different sources. Romanishin (1990) compared the Hα + [N II] photometry of 18 galaxies in common between his survey and Kennicutt & Kent (1983) and found that his equivalent widths were higher by 17% on average. A comparison of 32 galaxies in common between Kennicutt (1992) and Kennicutt & Kent (1983) shows a similar scale difference of 16%. We suspect that the discrepancy is due to a systematic problem in the continuum calibration and subtraction in the Kennicutt & Kent (1983) photometry, introduced perhaps by the presence of the telluric O_2 B absorption feature in their red continuum sideband. For this analysis we have corrected the Kennicutt & Kent (1983) equivalent widths and fluxes by a factor 1.16, to bring them into accord with the more recent measurements.

3. COLOR AND Hα SYNTHESIS MODELS

3.1. *Calculation of Models*

The luminosity, colors, and emission-line fluxes from evolving populations of stars were modeled with a weighted sum of contributions from stars with different masses and ages. We followed the basic procedure described in K83, but with improved stellar evolution models and ionizing fluxes. The key ingredients in the models are the stellar evolutionary tracks which describe the luminosity, effective temperature, and mass of a star as a function of initial mass and age, atmosphere models which allow the transformation from effective temperature and surface gravity to colors and ionizing photon production rates, the IMF, and a star formation history for the system to define the relative weights of different stellar ages.

The galaxy models presented here are based on the recently published stellar evolutionary tracks of Schaller et al. (1993, hereafter SSMM) for solar metallicity, and incorporating the effects of stellar mass loss These stellar evolutionary models are considerably improved over those used in K83, with updated opacities and reaction rates, and improved treatment of convection, convective overshooting, and mass loss. Our models also include a more detailed treatment of the shorter but essential late stages of evolution. For stars above 20 $M_\odot$ SSMM published two sets of tracks, with post–sequence mass-loss rates differing by a factor of 2. We found that the aggregate properties of the model galaxies are insensitive to this difference for most parameters. Models based on the tracks with

boosted mass-loss rates have very similar colors and about 3% less ionizing flux relative to the base models presented here. For the mass range 0.8–2.5 $M_\odot$ the SSMM calculations end at the helium flash, so horizontal branch evolutionary tracks from Seidel, Demarque, & Weinberg (1987) were appended. ZAMS points for stars less massive than 0.8 $M_\odot$ were extrapolated from the earliest age points in the lowest mass tracks, purely for convenience in distributing weights. Interpolated tracks were constructed for stars of intermediate mass, in order to provide smoother evolution in the predicted colors as a function of galaxy age.

The theoretical L_{bol}, T_{eff}, and mass at each evolutionary stage were transformed to fluxes in the *UBV* and Cousins *RI* passbands using the color table for the Revised Yale Isochrones, as described by Green (1988). The number of ionizing photons produced in the lifetime of a massive star was calculated using the emergent fluxes from Kurucz (1992) model atmospheres, in a manner similar to that used by Leitherer (1990) for a different set of evolutionary tracks. With appropriate weighting from the IMF, these were summed to give the ionizing output per mass of star formation. The corresponding Hα luminosity and equivalent width were calculated using the recombination rates for a 10,000 K gas (Hummer & Storey 1987), and the absolute calibration of the Cousins *R* magnitude from Bessell (1979).

The colors and Hα properties of a stellar population with a given IMF were computed as a function of age to form a "burst model." Burst models were computed for the IMFs of Salpeter (1955), Miller & Scalo (1979), K83, and Scalo (1986). Lower the upper stellar mass limits of 0.1 and 100 $M_\odot$ were adopted in all cases. Many of these IMFs can be approximated as power laws of the form:

$$\psi(m) = am^{\Gamma} d(\log m) . \quad (1)$$

In this notation the Salpeter IMF is a single power law with $\Gamma = -1.35$, while the Miller & Scalo (1979) function can be fitted by $\Gamma = -0.4$(0.1–1 $M_\odot$); -1.5(1–10 $M_\odot$); and -2.3 (10–100 $M_\odot$). The K83 IMF is identical to the Miller & Scalo function for $M < 10\ M_\odot$, with the $\Gamma = -1.5$ slope extended to 100 $M_\odot$; hence it is similar to the Salpeter IMF above 1 $M_\odot$, but takes into account the rollover in IMF at lower masses which is observed in the solar neighborhood. Scalo (1986) lists three parameterizations of the solar neighborhood IMF, which differ in the normalization of the function near the disk turnoff and depend on the presumed age and star formation history of the disk. These cannot be easily approximated with power laws, so we used the functions tabulated by Scalo (1986) directly. Models were computed for all three Scalo IMFs, but since they differ primarily in their normalizations above 1 $M_\odot$, the photometric properties of the respective galaxy models are very similar, and we tabulate only the results for the best-fitting intermediate IMF, which we denote henceforth as the "S86" IMF.

Model galaxies were constructed by summing together burst models with different ages, weighted by the star formation history of the population. Following the usual convention we parameterized the star formation history as an exponential function:

$$R(t) = R_0 \exp(-t/\tau) , \quad (2)$$

with a fixed disk age of 10 Gyr. For subsequent analysis each model was parameterized in terms of the birthrate parameter *b* of Scalo (1986), which is defined as the ratio of the SFR at the current time to the past SFR averaged over the age of the disk. This exponential model is reasonable for galaxies with constant or declining SFRs ($b \leq 1$), but galaxies with very high SFRs are generally the result of recent star formation bursts, rather than an exponentially increasing SFR over the lifetime of the disk. Consequently for $b \gg 1$ we computed a second set of models consisting of an instantaneous burst superposed on a steady state ($b = 1$) disk.

Table 1 lists the resulting colors and Hα EWs for a grid of 10 Gyr old model disks, for the Salpeter, K83, and S86 IMFs. Also listed are the values of τ and *b* for each model. These are used in § 5 to estimate values of the birthrate parameter *b* for disks of known color and Hα EW. For $b > 1$ two sets of values are listed, corresponding to the pure exponential and constant SFR + burst models described above. To illustrate the effect of the various model input parameters, Figure 1 compares *b* versus $B-V$ color relations from this paper with those used previously by Kennicutt (1983). The solid and dot-dashed lines show the relations from Table 1, for 10 Gyr old (pure exponential) disks and a K83 IMF (*solid*) and S86 solar neighborhood IMF (*dot-dashed*). The other two curves are relations from the older synthesis models described in Kennicutt (1983), using the K83 IMF and disk ages of 10 Gyr (*dotted line*) and 15 Gyr (*dashed line*). Figure 1 illustrates the sensitivity of the disk colors to several parameters, the disk age, IMF, and the stellar tracks used in the models. Hence it is not surprising that the colors are a relatively inaccurate tracers of the stellar birthrate history.

3.2. *Ionization Properties*

The most relevant parameter for the determination of SFRs is the ratio of ionizing photon luminosity (or Hα luminosity) to the total mass in formed stars. This is listed in Table 2 for several IMFs. Tabulated are the form of the IMF, the lower and upper stellar mass limits (M_l and M_u, respectively), the ionization rate per solar mass of stars formed [$Q(H^\circ)/m$], the Hα luminosity per solar mass [L(Hα)/SFR], and the ratio of this emissivity to that produced by the K83 IMF. These values are calculated for galaxies with continuous star formation (i.e., no change in the SFR over timescales comparable to the lifetimes of the oldest ionizing stars, $\sim 10^7$ yr), and without extinction effects or [N II] emission included. Ionizing fluxes are

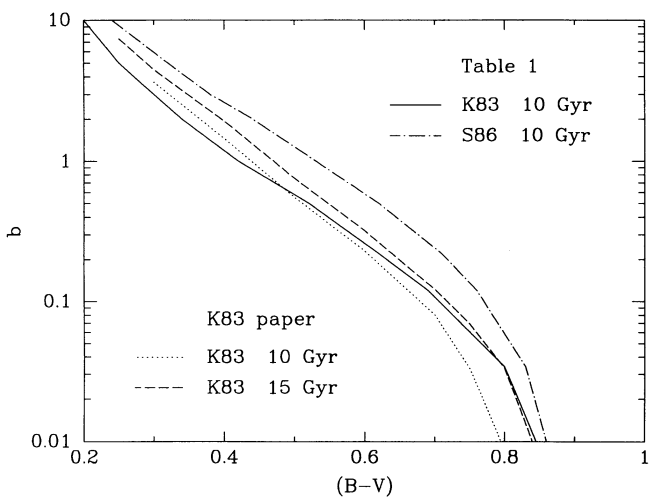

FIG. 1.—Relation between Scalo birthrate parameter *b* and $B-V$ color, for various disk models.

TABLE 1

SYNTHETIC GALAXY PROPERTIES

IMF	τ (Gyr)	b	$U-V$	$B-V$	M_V[a]	$V-R$	$R-I$	$(M/L)_B$	EW($H\alpha$) (Å)
K83	1	0.00045	0.46	0.88	6.31	0.51	0.53	4.79	0.78
	2	0.034	0.33	0.80	6.15	0.48	0.50	3.87	3.41
	3	0.12	0.19	0.69	5.94	0.44	0.47	2.89	10.6
	4	0.22	0.10	0.62	5.77	0.41	0.45	2.32	16.8
	8	0.50	−0.01	0.52	5.44	0.37	0.41	1.55	29.0
	∞	1.0	−0.10	0.42	5.06	0.32	0.38	1.00	42.5
	−6.3	2.0	−0.17	0.34	4.61	0.28	0.34	0.61	58.1
	−3.5	3.0	−0.21	0.30	4.31	0.26	0.32	0.45	68.4
	−2	5.0	−0.25	0.25	3.94	0.23	0.31	0.31	82.4
	−1	10	−0.31	0.20	3.45	0.20	0.28	0.18	106
	∞	2.0	−0.18	0.40	4.99	0.31	0.37	0.92	80.7
	∞	3.0	−0.25	0.37	4.93	0.30	0.36	0.85	115
	∞	5.0	−0.35	0.34	4.81	0.28	0.35	0.74	175
	∞	10	−0.49	0.27	4.56	0.25	0.33	0.56	286
Salpeter	1	0.00045	0.49	0.91	6.87	0.54	0.59	8.30	0.08
	2	0.034	0.34	0.82	6.72	0.51	0.56	6.65	5.24
	3	0.12	0.17	0.71	6.50	0.47	0.52	4.88	16.2
	4	0.22	0.07	0.63	6.32	0.43	0.49	3.86	25.6
	8	0.50	−0.06	0.51	5.97	0.38	0.45	2.52	44.0
	∞	1.0	−0.15	0.41	5.58	0.33	0.40	1.60	63.8
	−6.3	2.0	−0.22	0.33	5.11	0.28	0.36	0.96	86.0
	−3.5	3.0	−0.26	0.29	4.80	0.26	0.34	0.70	100
	−2	5.0	−0.30	0.24	4.41	0.24	0.32	0.47	119
	−1	10	−0.37	0.19	3.89	0.21	0.30	0.28	151
	∞	2.0	−0.25	0.38	5.49	0.32	0.39	1.43	119
	∞	3.0	−0.33	0.35	5.40	0.30	0.38	1.29	167
	∞	5.0	−0.43	0.31	5.25	0.28	0.36	1.08	247
	∞	10	−0.57	0.24	4.94	0.24	0.33	0.76	385
S86	1	0.00045	0.48	0.89	6.02	0.52	0.53	3.72	0.02
	2	0.034	0.39	0.83	5.89	0.49	0.51	3.15	0.91
	3	0.12	0.30	0.76	5.75	0.47	0.49	2.59	2.95
	4	0.22	0.24	0.71	5.64	0.45	0.47	2.24	4.90
	8	0.50	0.14	0.62	5.43	0.41	0.44	1.68	9.48
	∞	1.0	0.06	0.53	5.17	0.37	0.41	1.22	15.3
	−6.3	2.0	−0.03	0.44	4.84	0.32	0.37	0.83	23.6
	−3.5	3.0	−0.07	0.38	4.62	0.29	0.34	0.64	30.3
	−2	5.0	−0.12	0.32	4.34	0.26	0.31	0.47	39.6
	−1	10	−0.20	0.24	3.96	0.22	0.28	0.31	57.2
	∞	2.0	0.00	0.51	5.14	0.36	0.40	1.17	27.6
	∞	3.0	−0.04	0.50	5.11	0.35	0.40	1.13	39.3
	∞	5.0	−0.12	0.47	5.06	0.34	0.39	1.04	59.7
	∞	10	−0.25	0.42	4.94	0.32	0.38	0.89	97.6

[a] For one solar mass of star formation over 10 Gyr.

TABLE 2

SUMMARY OF IONIZATION PROPERTIES

Tracks	IMF	M_l	M_u	$Q(H_0)/m$[a]	L(Hα)/SFR[b]	Q/Q(K83)
SSMM93	K83	0.1	100	3.13	1.36	1.00
	Salpeter	0.1	100	2.91	1.26	0.93
	KTG93	0.1	100	1.30	0.56	0.42
	S86 (1)	0.1	100	0.39	0.17	0.12
	S86 (2)	0.1	100	1.07	0.46	0.34
	S86 (3)	0.1	100	1.93	0.84	0.62
K83[c]	K83	0.1	100	2.57	1.12	0.82
MM89[d]	K83	0.1	100	4.10	1.78	1.31
	Salpeter	0.1	100	3.98	1.72	1.27

[a] Units 10^{60} photons $M_\odot^{-1}$.
[b] Units $(10^{41}$ ergs s$^{-1})/(M_\odot$ yr$^{-1})$.
[c] Tracks used in models of Kennicutt 1983.
[d] From photoionization models of Leitherer 1990.

listed for all three parameterizations of the Scalo (1986) IMF (best fit and upper/lower limits of the IMF slope). We also list results for the recently published solar neighborhood IMF of Kroupa, Tout, & Gilmore (1993; denoted KTG93), which uses the Scalo IMF for high-mass stars but rederives the IMF for $m < 1\ M_\odot$.

The last three entries in Table 2 list ionizing fluxes from previous results from K83 and Leitherer (1990), using the best stellar models that were available at the time. The new models yield ionizing luminosities per unit mass which are $\sim$20% higher than in the K83 models for the same IMF. The more recent stellar models have higher bolometric luminosities during the post–main-sequence phases and have slightly longer hydrogen burning lifetimes. This means that SFRs at a given Hα luminosity are 20% lower than derived by K83, but this is compensated in part by the 16% increase in the Hα flux scale (§ 2), so that our net SFRs are only 5% lower than those derived by K83 for the same galaxy and assumed IMF. On the other hand, the ionizing fluxes per unit mass derived here are 31% *lower* than those derived by Leitherer (1990) using the stellar evolution models of Maeder & Meynet (1989; MM89). This illustrates the sensitivity of the extragalactic SFR scale to the stellar input data, though extinction and IMF uncertainties remain the largest sources of error in these SFR scales.

4. THE IMF IN STAR-FORMING DISKS

The integrated Hα equivalent width (EW) is sensitive to the ratio of ionizing stars to lower mass red giant stars, so it can serve as a diagnostic of the IMF slope between $\sim$1 and 30 $M_\odot$. Following 1983 we used the relation between Hα EW and broad-band color to constrain the mean IMF in star forming disks.

Figure 2 shows the correlation between integrated Hα + [N II] EW and face-on corrected $(B-V)_T^0$ color (RC3) for our sample. Superposed on the data are two sets of evolutionary synthesis models, with a K83 IMF (*left*) and the "best fit" S86 IMF (*right*). Each line represents a locus of models with fixed age (10 Gyr), IMF, and stellar mass range (0.1–100 $M_\odot$), but with variable birthrate parameter b, as interpolated from Table 1 with [N II]/Hα = 0.5. The dashed line in each panel shows an extinction-free model, while the solid line shows the same model with the EWs reduced by a factor of 2 to account for extinction, and the colors reddened by 0.05 mag, as discussed below.

The effects of extinction on the EWs and colors are difficult to model precisely. Dust will tend to reduce the Hα line emission, weaken the underlying red continuum, and redden the $B-V$ colors, but the net effect on the EWs and color is complicated by the patchy nature of the extinction and the different stellar mixes at Hα, B, V, and R. The mean extinction of Hα line emission can be estimated from radio continuum observations or optical spectroscopy of individual H II regions, and averages 1–1.5 mag for most spirals (Israel & Kennicutt 1980; van der Hulst et al. 1988; Oey & Kennicutt 1993). This is consistent with the mean extinction determined from thermal radio continuum and Hα fluxes of entire disks (Israel & van der Hulst 1983; K83). The extinction in the stellar continuum can be determined by modeling the light distribution, and recent work suggests that the face-on extinction at R is low, a few tenths of a magnitude or less (Byun 1992). Hence, the net effect of extinction will be to reduce line emission relative to the underlying red continuum. The same observations imply that the reddening of the integrated face-on colors should be small, $\leq$0.1 mag in most cases. The solid lines in Figure 2 show our

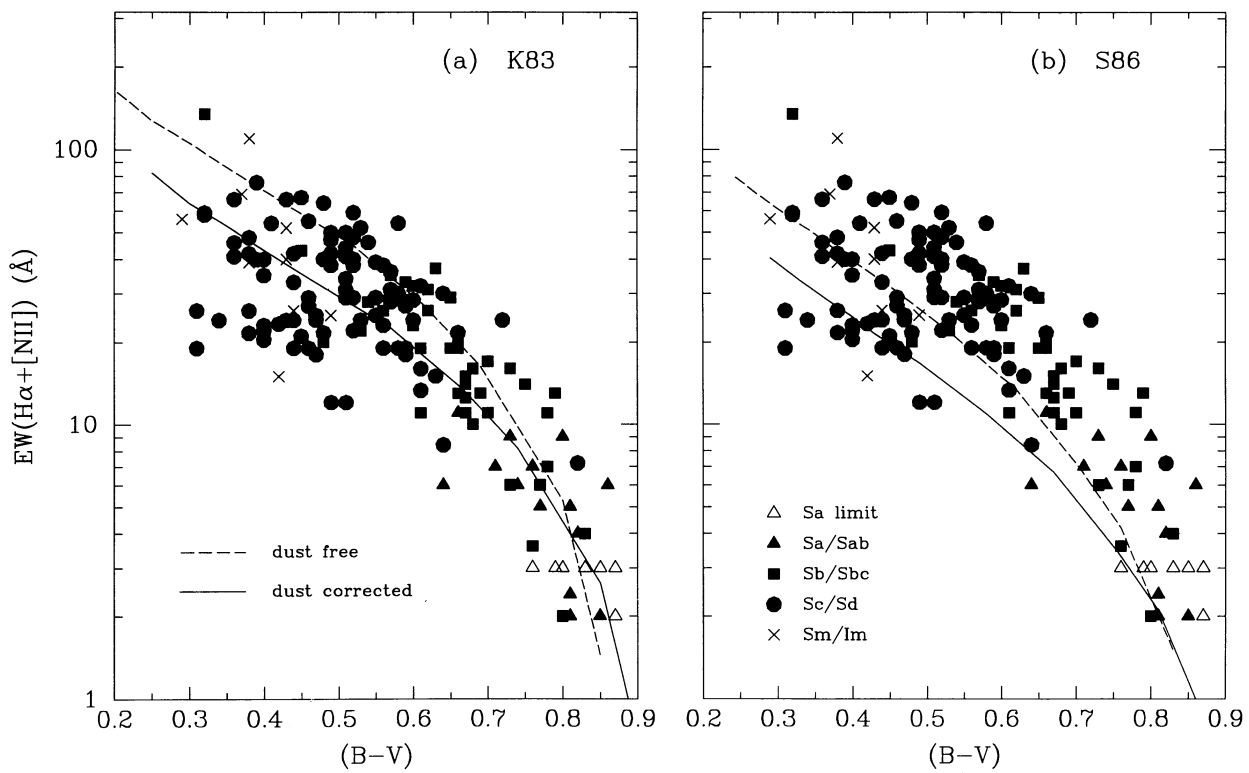

FIG. 2.—Relation between emission-line equivalent width for our sample, with disk models superposed, using a K83 IMF (*a*) and the S86 IMF (*b*). Dashed lines show extinction-free models. Solid lines denote models with approximate corrections applied for extinction and reddening, as described in the text.

best-estimate model, with a mean extinction in the Hα EW of a factor 2, and a net reddening of the corrected RC3 colors of 0.05 mag. The reddening and Hα extinction probably vary considerably among the galaxies observed, but we believe that the two cases shown in Figure 2 should bracket the range of extinction effects for most of the sample.

The K83 IMF (Fig. 2*a*) or a Salpeter IMF (not shown) provide reasonable fits to the observed EW–color relation. This is consistent with several previous studies (K83; Gallagher et al. 1984; Buat, Donas, & Deharveng 1987). However, the S86 IMF (Fig. 2*b*) appears to be deficient in massive stars by a factor of ~1.5–2.5, depending on the extinction model employed. This result holds for all fits to the local IMF in Scalo (1986), because the photometric properties of the respective models are similar. However, the total stellar mass per unit ionizing luminosity differs substantially between the three normalizations; relative to the K83 IMF the SFRs per unit Hα flux are 2.1, 3.9, and 8.3 times higher for the three Scalo IMFs (see Table 2). The latter values would imply SFRs in nearby galaxies which are clearly inconsistent with their measured disk masses and ages.

We conclude that the photoionization properties of nearby galaxies are consistent with a mean IMF slope above 1 $M_\odot$ of $\Gamma \simeq -1.35$ to -1.5 (Salpeter or K83, respectively). This is significantly shallower than recent determinations of the solar neighborhood IMF, which range over $\Gamma \simeq -1.7$ to -2.3 over the same mass range (Miller & Scalo 1979; Scalo 1986). It would appear that these local IMFs underpredict the ionizing luminosities of external galaxies by factors of 2–8, depending on the low-mass normalization.

What is the explanation for this inconsistency? We doubt that it can be attributed to errors in the Hα observations, the synthesis models, or the extinction corrections employed. Potential systematic errors which have not been considered, such as the escape of ionizing photons from spiral disks, or the presence of heavily obscured SFRs would only increase the discrepancy with steep IMF models. The observed EWs and colors can be reconciled with the solar neighborhood IMF only if disks are virtually extinction-free, and we adopt the most top-heavy IMF that is marginally consistent with the observations, i.e., if we push every model parameter to its limit.

Instead we suspect that the discrepancy is genuine, reflecting either a difference in the upper IMF between the Galaxy and the late-type galaxies in Figure 2, or else a deficiency of massive stars in the small volume of the Galaxy which has been used to construct the local IMF. The bulk of the massive star formation in late-type galaxies takes place in giant H II complexes (Kennicutt, Edgar, & Hodge 1989), and there is evidence that the upper IMFs in such regions may be significantly shallower than in the solar neighborhood (Parker & Garmany 1993). Hence, this explanation is at least a plausible one, but it needs to be tested with observations of a larger sample of OB complexes, both in our Galaxy and in nearby late-type disks.

Similar excesses in ionizing luminosity over that expected for a solar neighborhood IMF are observed in infrared-luminous starburst galaxies such as M82, and these are often attributed to a top-heavy IMF (Rieke et al. 1980, 1993; Joseph 1991; Bernlöhr 1992). Are we observing the same phenomenon in the disks of normal galaxies? Constraining the IMF in the IR-luminous starbursts is a considerably more complicated exercise, due to the heavy obscuration and the strong time dependence of the star formation burst. It is nevertheless instructive (if oversimplistic) to compare the ionizing luminosity and stellar mass budgets in the different classes of objects. In the best studied starburst region to date, M82, observations compiled by Rieke et al. (1993) yield a lower limit to the ionizing luminosity of 10^{54} photons s^{-1}, an upper limit in stellar mass of 2.5×10^8 $M_\odot$, and a burst age of ~20–50 Myr. Combining these parameters yields a mean ratio $Q(H^0)/m = 2.5\text{–}6 \times 10^{60}$ photons $M_\odot^{-1}$. Comparison with Table 3 confirms that these values are much higher than expected for a steady state starburst with an S86 IMF ($0.4\text{–}2 \times 10^{60}$ photons $M_\odot^{-1}$), but they are only slightly higher than expected with a K83 or Salpeter IMF ($\sim 3 \times 10^{60}$ photons $M_\odot^{-1}$). Hence part of the apparent anomaly in the IMFs of starburst galaxies relative to the solar neighborhood may simply reflect a deficiency of massive stars in the local neighborhood. If an IMF appropriate to the galaxies in our sample is used as a basis for modeling the starbursts, the need for extreme differences such as lower mass cutoffs in the 2–7 $M_\odot$ range may be partly alleviated (Bernlöhr 1992; Rieke et al. 1993).

TABLE 3

ADOPTED M/L PARAMETERS[a]

Type	M_{tot}/L_B	M_{tot}/L_V	L_d/L_{tot}	M_d/L_V[b]	M_d^*/L_V[c]
Sa/Sab	3.2	3.2	0.65	2.1	1.1
Sb	3.2	3.3	0.78	2.6	1.3
Sbc/Sc	2.4	2.8	0.86	2.6	1.3
Scd/Sd	2.0	2.6	1.00	2.6	1.3
Sm/Im	0.9	1.2	1.00	1.2	0.6

[a] Measured within D_{25}.
[b] Disk mass to total luminosity ratio.
[c] Stellar disk mass to total luminosity ratio.

5. STAR FORMATION HISTORIES OF DISKS

As discussed in § 2, the Hα EW and color of a disk can be used to measure the ratio of the current SFR to the average past SFR, the Scalo *b* parameter. The synthesis models in Table 1 yield relations between *b* and the broad-band colors (Fig. 1) or the extinction-corrected Hα EW (Fig. 3). If the absolute Hα luminosity is measured, *b* can also be estimated by comparing the current SFR with the total stellar mass of the disk divided by its age. Each of these methods has distinct

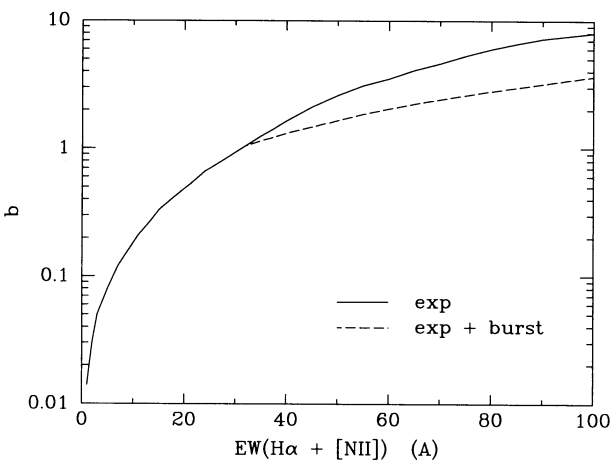

FIG. 3.—Relation between Scalo birthrate parameter *b* and Hα emission line equivalent width, from the models in Table 2. The solid line is for an exponential star formation history and K83 IMF; the dashed line is for an exponential plus burst model as described in the text.

advantages and limitations, so it is useful to compare the results from each.

5.1. *Determination of Birthrate Parameters*

K83 measured b for 116 galaxies by comparing the Hα-derived current SFRs with their mean past SFRs, as determined from the mass and age of the stellar disks. Formally,

$$b \equiv \frac{\mathrm{SFR}}{\langle \mathrm{SFR} \rangle_{\mathrm{past}}} = \frac{\mathrm{SFR} \cdot \tau_d}{M_d} (1 - R) , \qquad (3)$$

where M_d and τ_d are the stellar mass and age of the disk, respectively, and the return fraction R is the fraction of mass in a stellar generation that is returned to the disk over its lifetime (Tinsley 1980). This method takes advantage of the direct determination of the current SFR, and is less model-dependent than the other methods. Its primary drawback is that the stellar mass of a disk cannot be measured directly, but rather must be estimated using the disk luminosity and an average M/L ratio for galaxies of a given type. Measured M/L ratios vary considerably, even among galaxies of the same type (e.g., Kent 1986), and they will vary systematically with the birthrate history itself. Hence, values of b derived in this way will have significant random errors, but mean birthrates for large samples of galaxies should be more reliable.

To apply this method to the current sample, we converted the extinction-corrected Hα + [N II] luminosities to current SFRs (Table 2), using a K83 IMF, a distance scale with $H_0 = 75$ km s^{-1} Mpc^{-1}, and a mean [N II]/Hα ratio of 0.5. Average past SFRs were determined from the observed V luminosity of each galaxy, using the M/L ratios listed in Table 3, and assuming a disk age of 10 Gyr. The M/L values were taken from Faber & Gallagher (1979), and converted to our distance scale, to the R_{25} radius, and from L_B to L_V, to reduce the sensitivity to stellar population variations. These in turn were converted to *disk* M/L ratios, using the mean bulge/disk ratios from Simien & de Vaucouleurs (1986), or when available the published bulge/disk ratio for the galaxy in question (see § 5.2). Finally, the ratios were multiplied by 0.50 to correct for the average dark matter contribution within the R_{25} radius (Rubin 1987). The final adopted stellar M_{disk}/L_V ratios are listed in the last column of Table 3. The birthrate parameter then follows from equation (3), using $R = 0.4$ (see § 6.2). The number of steps listed above serves to emphasize the considerable uncertainty in b derived with this method.

An alternative means of measuring b is to use the EW(Hα) versus b relation from the synthesis models. This method also takes advantage of the linear dependence of the Hα flux on the SFR, but it is distinct from the previous method in that it relies on the accuracy of the evolutionary synthesis model, rather than on average empirical M/L ratio for a given galaxy type. For galaxies with smooth star formation histories this provides the most accurate measurement of b, because the dependence of M/L on b is implicitly included in the model. It is less reliable for galaxies with high SFRs, however, because the EW versus b calibration is sensitive to the form of the star formation history. This is illustrated in Figure 3, which compares the EW versus b relation for the exponential + burst approximation described in § 3.1 (*dashed line*) with a pure exponential model (*solid line*). The latter model is unrealistic for active galaxies, because it assumes that the SFR has increased steadily over the past 10 Gyr. This causes the value of b to be overestimated for a given EW, because the exponential model overpredicts the strength of the continuum underlying Hα (cf. Fig. 3). Figure 4 compares values of b derived the observed EW(Hα) with the exponential + burst model with those derived from the observed Hα luminosity and M/L ratios and shows that there is reasonable consistency between the two scales. Based on these results we have used the exponential + burst approximation to estimate b from the EWs.

As a final check, we applied the $B-V$ versus b relation in Figure 1 to derive birthrate parameters for each galaxy. This is the least reliable of the methods, because the derived birthrates are very sensitive to small errors in the colors (or the color

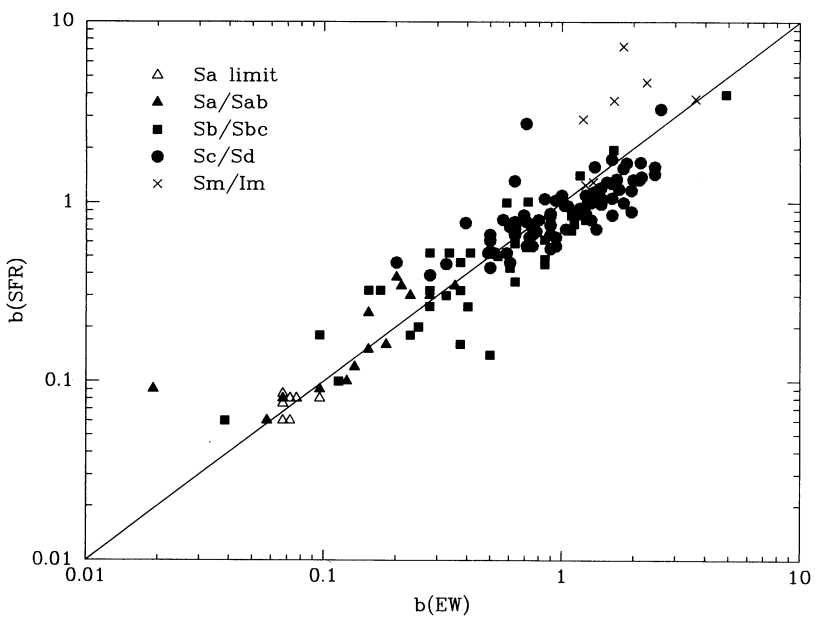

FIG. 4.—Comparison of disk birthrate parameters derived from the model EW vs. b relation with those derived from comparison of current SFRs and disk masses.

models) and are subject to large systematic errors from reddening, metallicity variations, and bulge contamination. There is no easy way to correct for these effects, especially when only integrated colors (disk + bulge) are available. Figure 5 compares b values derived from $(B-V)_T^0$ colors with those derived from the Hα luminosities. In this comparison both b's refer to the entire galaxy (spheroid and disk), because only integrated colors are available. There is reasonable consistency for the late-type galaxies, but the scatter in $b(B-V)$ is very large, and there is a systematic difference in the early-type systems, where the sensitivity to reddening, age, and metallicity effects is especially severe. Including a mean face-on reddening correction of only a few hundredths of a magnitude would bring the two birthrate scales into accord. In view of these large uncertainties this method was not used in the remainder of the analysis.

5.2. *Results*

Mean values of the birthrate parameter b were calculated for each galaxy in our sample, by averaging the values derived from the Hα EWs and luminosities (when available). Since we are interested in the evolutionary properties of disks, the integrated EWs and galaxy magnitudes were corrected for bulge contamination, under the assumption that all of the line emission is produced in the disk (including the nucleus). A search of the literature produced bulge/disk (B/D) ratios for 63 galaxies, mostly from the compilation of Simien & de Vaucouleurs (1986). When photometry was available at more than one wavelength we adopted the measurement closest to Hα. Otherwise we ignored the small color dependence of the B/D ratio. In addition the sample contains 29 Sd, Sm, and Im galaxies, which can be safely treated as pure-disk systems. For the other 118 spirals in the sample we adopted the mean B/D values for each galaxy type as compiled in Simien & de Vaucouleurs. The mean disk fractions range from 0.65 in Sa galaxies to 0.90 in Sc galaxies, so the corrections are important only in early-type systems.

TABLE 4

MEDIAN BIRTHRATE PARAMETERS

Type	EW(Hα)	L(Hα)	$(B-V)^a$	Average[b]
Sa	<0.07	<0.08	<0.02	<0.07
Sab	0.17	0.16	0.06	0.17
Sb	0.37	0.33	0.12	0.33
Sbc	0.88	0.85	0.27	0.84
Sc	1.04	0.95	0.57	0.99
Scd/Sd	0.63	0.75	1.02	0.69
Sm/Im	1.31	3.70	1.33	1.67

[a] Includes bulge contribution.
[b] Distribution of average b from EW(Hα) and L(Hα).

Figure 6 shows the distribution of b for the disks in our sample, subdivided by galaxy type. Normal and barred galaxies are combined, as there is no evidence that they differ systematically in their integrated SFRs (Kennicutt 1993; Ryder 1993). In each panel the hatched histograms denote galaxies with individual measured B/D ratios, where the disk separation should be accurate, or Scd–Im galaxies with no bulges. The open histograms show the distribution for the entire sample. Table 4 lists the median values of b for each subtype, for each of the three methods described above, as well as for the average b derived from the Hα EWs and luminosities. Although there are scale differences between the methods, the type-dependent trend is confirmed in all of the methods. For many of the Sa galaxies only upper limits to b are determined, so the average listed for that type are upper limits as well.

Figure 6 and Table 4 show a smooth progression in the star formation history with Hubble type, with the ratio of current to average past SFR increasing from 0.01–0.1 in Sa disks to 0.5–2 in a typical Sc disk. This is consistent with the long-standing qualitative interpretation of the integrated colors and

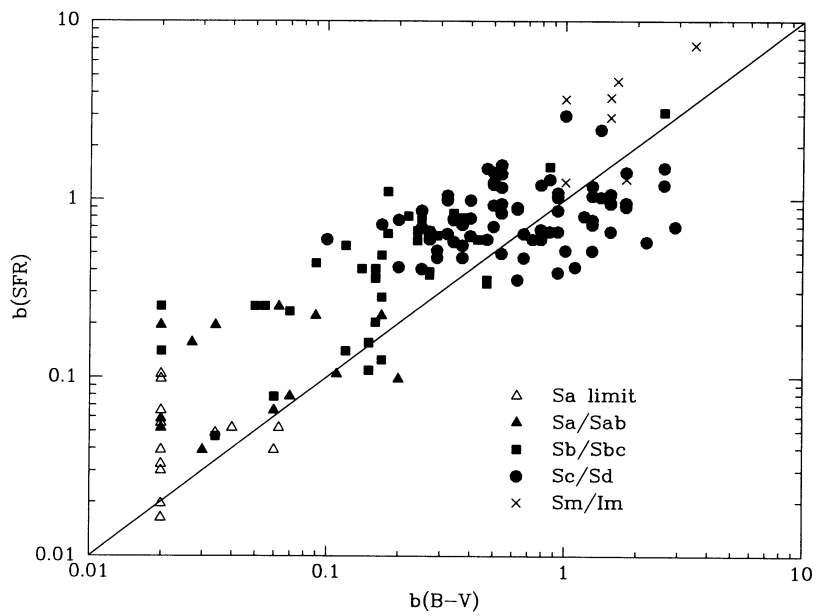

FIG. 5.—Comparison of integrated birthrate parameters derived from the model color vs. b relation with those derived from comparison of current SFRs and galaxy masses. These values are based on integrated magnitudes, which are affected by bulge contamination. This is responsible for the systematic differences among early-type galaxies.

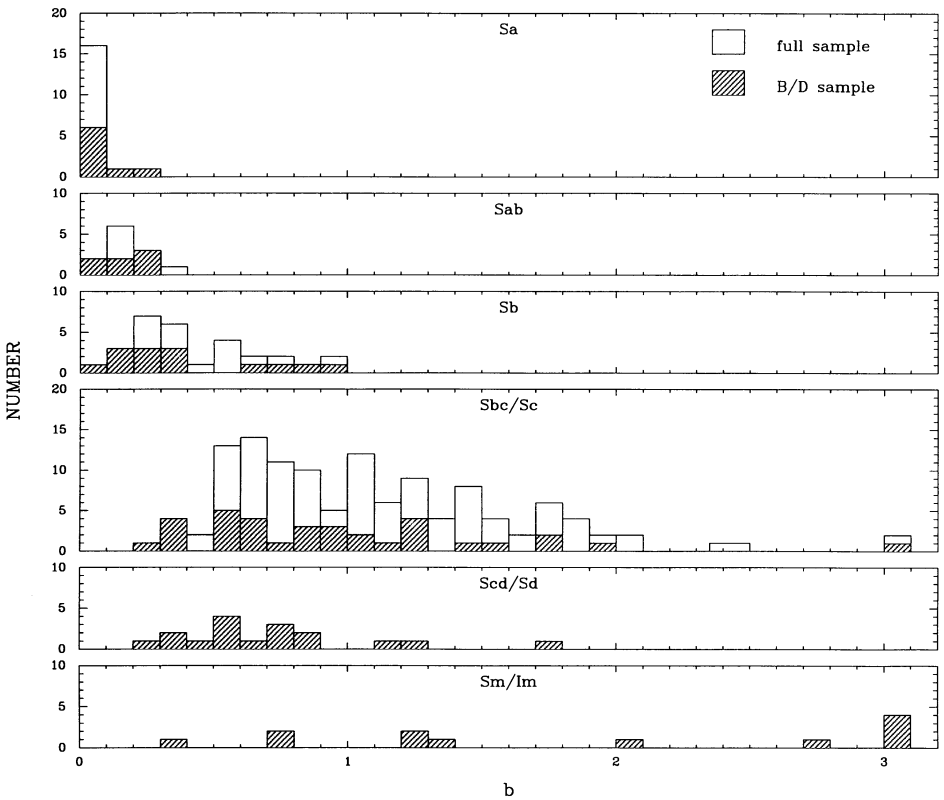

FIG. 6.—Distribution of disk birthrate parameter b, the ratio of the current SFR to the average past SFR, for our sample. Hatched data include galaxies with individually measured bulge/disk ratios. Open histograms include all galaxies in the sample.

emission-line properties of spirals along the Hubble sequence (Searle et al. 1973; Larson & Tinsley 1978; Kennicutt 1983; Gallagher et al. 1984) and shows unequivocally that the trends in integrated properties are primarily due to changes in the evolutionary properties of *disks*, rather than changes in the bulge/disk ratio. Between types Sc and Sa, for example, the mean ratio of current to past SFR in the disk decreases by at least a factor of 20, whereas the disk fraction decreases by only 25% (from ~90% to 65%). It is possible that the changes in disk evolutionary may be causually related to changes in bulge/disk morphology, but it is the former that dominate the trends in photometric properties along the spiral sequence.

It is interesting that the general gradient in star formation properties appears to be broken by the Sd galaxies. Although the Scd/Sd sample is small (17 objects), the Hα-derived b values differ by $\sim 5\ \sigma$ in the means between types Sc and Scd/Sd. It may be that the classification criteria for the Sd class preferentially select galaxies with lower SFRs per unit area or unit disk mass. However this trend is not seen in the $B-V$ colors, so we cannot exclude the possibility that the difference is an artifact of small number statistics or other selection effects. The irregular galaxies in the sample (bottom panel of Fig. 6) show a very large dispersion in properties and a high mean b, but the latter may be an artifact of selection bias in the small sample. Instead we refer the reader to more complete analyses of irregulars by Gallagher et al. (1984) and Hunter & Gallagher (1985).

The strong trends apparent in Figure 6 should not be misinterpreted as implying that there are no early-type galaxies with galaxies with high SFRs. Many strongly interacting galaxies have high SFRs nearly independent of their Hubble type (e.g., Kennicutt et al. 1987), and samples of early-type systems with unusually blue colors (e.g., Pogge & Eskridge 1993) or strong *IRAS* emission (e.g., Devereux & Young 1991) often possess high absolute SFRs. Our conclusions apply to normal, optically selected galaxies, and specifically exclude interacting and/or peculiar systems.

5.3. *Discussion*

From an observational point of view the progression in disk star formation histories with morphological type is not surprising, since one of the fundamental classification criteria is disk resolution, which should relate at least indirectly to the fraction of young stars in the disk. However, the physical explanation for this trend is not at all clear, at least within the context of the conventional closed-box disk evolution picture. The higher SFRs per unit luminosity in late-type disks today are consistent with their higher fractional gas content (e.g., Young 1990; Roberts & Haynes 1994), but if disks evolve as closed systems their *initial* gas densities should have been comparable for all types. What initial condition in the Sa disks caused them to form stars over a timescale which was an order of magnitude shorter than for Sc disks? It is tempting to speculate that Sa disks may have possessed higher initial gas densities, but if this were the case we would expect present-day Sa galaxies to have much higher stellar surface densities than Sc disks (not observed), and we would expect to see strong radial variations in the birthrate histories of all exponential disks (also not observed). If gas density were the dominant parameter controlling the timescale for star formation, why did the

outer, low-density regions of Sa–Sb galaxies convert their gas to stars much more rapidly than the inner, high-density regions of Sc galaxies?

This paradox suggests that some other mechanism is needed to account for the strong type dependence of disk birthrate histories. Star formation thresholds offer an attractive means of abruptly curtailing the stellar birthrate when the gas density approaches the Jeans's density (Quirk 1972; Kennicutt 1989). If early-type galaxies represent systems which recently reached this threshold, the abrupt drop in the SFR below the threshold density would magnify smaller initial differences in the relative SFRs along the Hubble sequence. An alternative possibility is that the disks have grown slowly by accretion of gas, and the differences in the birthrate histories mimic underlying differences in the accretion histories of disks (e.g., White & Frenk 1991).

6. GAS CONSUMPTION TIMESCALES

The future timescale for star formation in a disk can be derived by comparing the current SFR to the available interstellar gas mass. Roberts (1963) first performed such an analysis, using rough estimates of the SFRs and H I masses of nearby galaxies. Following the convention introduced by Sandage (1986) we define a "Roberts time" τ_R:

$$\tau_R \equiv \frac{M_{\rm gas}}{\rm SFR} \tag{4}$$

As pointed out by Roberts, the actual timescale for gas depletion is longer than given by this equation, because corrections need to be applied for gas recycling and the future time dependence of the SFR. Most recent discussions of gas depletion times (Larson et al. 1980; Kennicutt 1983; Sandage 1986; Donas et al. 1987; Larson 1992) have ignored the recycling correction or applied a modest correction factor (~25%), following Tinsley (1980). For simplicity, we first discuss the distribution of uncorrected τ_R in § 6.1 and discuss the recycling correction separately in § 6.2.

6.1. *Distribution of Roberts Times in Nearby Spirals*

Integrated H I and molecular gas masses are available for 63 galaxies in our sample, including 40 field galaxies and 23 Virgo Cluster members. Most of the data were taken from the compilation of Young et al. (1989). These were supplemented with CO measurements of M31 by Koper et al. (1991) and 18 other galaxies by Sage (1993). These were converted to H_2 masses using the conversion factor of Young et al. (1989), a factor 1.4 to include helium and heavy elements, and were corrected to the distance scale used here. Note that while the absolute gas masses and SFRs are distance-dependent quantities, the gas consumption times are independent of distance.

Table 5 lists relevant data and derived Roberts times. Virgo Cluster members (V) and galaxies classified as interacting or peculiar (p) are noted in the last column of the table. Although we excluded very peculiar starburst galaxies (e.g., M82) from our sample, so as not to bias the results toward short gas consumption times, the sample still contains a few objects with abnormally high relative SFRs (e.g., NGC 3310, NGC 3353) and short Roberts times. Although we cannot claim to have compiled a completely unbiased sample for this analysis, we believe that the sample is large enough to be qualitatively representative of all but the lowest surface brightness systems.

Figure 7*a* (*top panel*) shows the distribution of τ_R for our sample, as taken from column (8) of Table 5. The median Roberts time for the entire sample is 3.6 Gyr. This compares well with mean times of 4–5 Gyr (including a 25% correction for recycling) derived previously by Larson et al. (1980) and Kennicutt (1983). The main difference in the present study is better SFRs and gas masses measured directly from H I and CO measurements, rather than scaled H I masses. The median

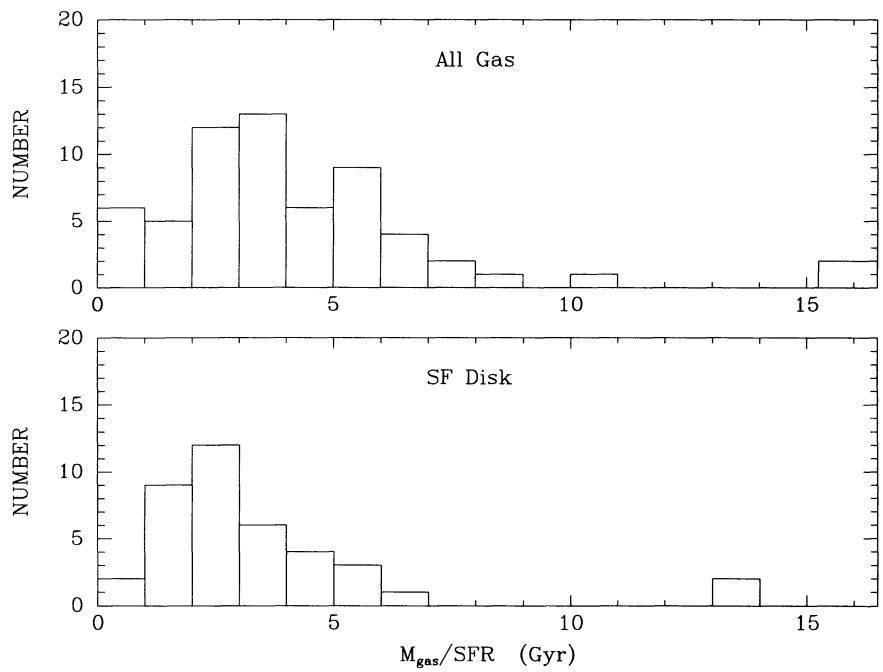

FIG. 7.—Distribution of Roberts gas consumption times for our sample. Values are uncorrected for stellar recycling. Times in the top plot were computed using the total gas masses. The bottom plot only includes gas located within the optical disk diameter.

TABLE 5

GAS MASSES AND CONSUMPTION TIMES

NGC (1)	Type (2)	Dist (Mpc) (3)	log $L_{H\alpha}$ (ergs s^{-1}) (4)	log $M_{H\,I}$ ($M_\odot$) (5)	log M_{H_2} ($M_\odot$) (6)	log M_{gas} ($M_\odot$) (7)	τ_R[a] (Gyr) (8)	$(\tau_R)_d$[a] (Gyr) (9)	Notes (10)
224.....	Sb	0.7	40.5	9.64	8.40	9.66	10.7	6.4	
628.....	Sc	11.5	41.46	10.22	9.43	10.29	4.9	2.0	
925.....	SBc	10.6	41.01	9.83	8.87	9.87	5.3	3.7	
1058.....	Sc	9.9	40.26	9.29	8.22	9.33	8.5	1.7	
1569.....	Sm	2.7	40.41	8.21	6.26	8.22	0.5		p
2276.....	Sc	35.3	41.77	9.77	10.03	10.22	2.1		p
2403.....	Sc	3.6	40.87	9.70	7.91	9.71	5.1	2.1	
2633.....	SBb	32.2	40.99	9.70	9.57	9.94	6.5		
2775.....	Sa	15.9	40.06	8.59	9.18	9.28	12.1		
2841.....	Sb	9.5	40.13	9.46	9.32	9.70	26.9	13.6	
2903.....	Sc	6.3	40.85	9.29	9.11	9.51	3.3	3.1	
3031.....	Sb	3.6	40.81	9.50	8.23	9.52	3.8	1.2	
3147.....	Sb	38.7	41.48	9.78	10.36	10.46	7.0		
3310.....	Sbc	14.3	41.56	9.59	8.52	9.63	0.9		p
3353.....	p	14.5	40.83	8.74	7.77	8.80	0.7		p
3368.....	Sab	10.1	40.61	9.23	9.13	9.48	5.5	4.6	
3504.....	SBb	19.7	41.29	8.63	9.21	9.31	0.8		
3521.....	Sb	8.4	>41.05	9.66	9.61	9.94	<5.6		
3623.....	Sa	8.8	40.01	8.43	<8.76	<8.93	<6.0		
3627.....	Sb	8.8	41.10	8.86	9.47	9.56	2.1		
3628.....	Sbc	8.8	>40.47	9.68	9.43	9.87	<18.5		
3690.....	Sp	41.3	42.29	<9.39	10.00	10.10	0.5		p
3893.....	Sc	13.7	41.11	9.53	9.04	9.65	2.5		
4192.....	Sb	17.5	41.16	9.81	9.50	9.98	4.9	3.0	V
4212.....	Sc	17.5	40.93	<8.33	9.23	9.28	1.6		V
4216.....	Sb	17.5	41.03	9.42	9.32	9.67	3.2	2.0	V
4254.....	Sc	17.5	41.72	9.87	10.00	10.24	2.4	2.0	V
4294.....	SBc	17.5	40.92	9.35	<8.30	9.39	2.1	1.3	V
4303.....	Sc	17.5	41.78	9.86	9.88	10.17	1.8	1.5	V
4321.....	Sc	17.5	41.58	9.54	10.05	10.17	2.8	2.8	V
4388.....	Sab	17.5	41.03	8.81	8.89	9.15	1.0	1.0	V
4394.....	SBb	17.5	40.3	8.70	8.97	9.16	5.5	5.5	V
4402.....	Sb/Sc	17.5	40.16	8.71	9.32	9.42	13.1	13.1	V
4449.....	Sm	4.0	40.76	9.47	7.42	9.48	3.8		
4501.....	Sbc	17.5	41.33	9.39	9.87	9.99	3.3	3.3	V
4535.....	SBc	17.5	41.20	9.89	9.72	10.11	6.0	3.5	V
4548.....	SBb	17.5	40.88	9.16	9.26	9.51	3.1	2.3	V
4569.....	Sab	17.5	41.01	8.80	9.70	9.76	4.0	4.0	V
4571.....	Sc	17.5	40.56	8.97	9.10	9.34	4.4	4.3	V
4579.....	Sab	17.5	41.09	8.86	9.48	9.57	2.2	2.2	V
4631.....	Sc	8.0	41.20	10.07	8.89	10.10	5.8		
4639.....	SBb	17.5	40.73	9.13	<8.37	9.20	2.2	1.3	V
4647.....	Sc	17.5	40.85	8.81	9.30	9.42	2.7	2.7	V
4651.....	Sc	17.5	41.09	9.69	9.07	9.78	3.6	1.7	V
4654.....	SBc	17.5	41.18	9.63	9.39	9.83	3.2	2.5	V
4689.....	Sc	17.5	40.78	8.78	9.37	9.47	3.6	3.6	V
4713.....	SBc	17.5	41.27	9.64	<8.37	9.66	1.8	0.6	V
4736.....	Sab	4.6	40.65	8.52	8.63	8.88	1.2	1.2	
4808.....	Sc	17.5	40.99	9.68	<8.52	9.73	4.0		V
4826.....	Sab	4.7	40.17	8.35	8.63	8.81	3.2	2.1	
5055.....	Sbc	7.3	>41.00	9.70	9.67	9.99	7.1	5.9	
5194.....	Sbc	7.2	41.44	9.42	9.94	10.05	3.0	3.0	p
5236.....	SBc	5.0	41.57	9.96	9.96	10.26	3.6	2.2	
5457.....	Sc	6.0	41.46	10.28	9.66	10.37	6.0	6.0	
6207.....	Sc	13.1	40.73	9.15	8.15	9.19	2.1		
6503.....	Sc	4.0	40.01	8.77	8.23	8.88	5.4	1.8	
6574.....	Sbc	32.2	41.3	9.08	9.79	9.87	2.6		
6643.....	Sc	23.2	41.44	9.75	9.41	9.91	2.2		
6946.....	Sc	5.0	41.08	9.69	9.35	9.85	4.3	2.5	
7217.....	Sb	16.5	40.9	8.90	9.11	9.31	1.7		
7331.....	Sb	14.9	41.37	10.02	9.92	10.28	5.9	4.6	
7479.....	SBbc	35.1	41.39	10.03	10.06	10.35	6.6		
7817.....	Sbc	19.1	40.73	9.11	9.12	9.42	3.6		

[a] Roberts times uncorrected for stellar recycling.

NOTES.—(p) peculiar or interacting galaxy; (V) Virgo Cluster member.

values of τ_R for the field and Virgo subsamples are 4.0 and 3.2 Gyr, respectively, with the difference reflecting the well-known H I deficiencies in the Virgo spirals (e.g., Warmels 1988).

The timescales derived above assumed that all of the gas in disks is available for star formation, when in fact much of it lies far beyond the outer radii of the star forming disks. Consequently equation (4) overestimates the time required to deplete the gas in the inner disks, where star formation is currently taking place. Spatially resolved H I data are available for 39 of the galaxies (Warmels 1986), and these can be combined with the available CO masses (virtually all of which lies within the optical disk) to estimate τ_R for the optical disks (R_{25}) alone. The resulting consumption times are listed in column (9) of Table 5, and the distribution is shown in Figure 7*b* (*bottom panel*). These times, which more accurately reflect the star forming lifetime of the optical disk, are considerably lower, 2.7 Gyr in the median, with no significant difference between the field and Virgo subsamples (2.8 and 2.6 Gyr, respectively).

Figure 7 illustrates the gas consumption paradox raised by the previous analyses by Larson et al. (1980) and Kennicutt (1983). In the absence of recycling, most nearby spirals will exhaust the gas in their star forming disks on times ranging from 0.1 to 0.6 of the Hubble time, and less than a quarter of the Hubble time on average. For most late-type galaxies even these values are overestimates, because active star formation will be curtailed when the gas surface density is lowered to the Jeans's stability limit, which for most late-type disks is roughly half the current density (e.g., Kennicutt 1989). In that case the median timescale for Sc galaxies in our sample to transform to Sa–Sb galaxies is less than 2 Gyr! Such a coincidence in galactic timescales is highly improbable, so something must be wrong with the assumptions underlying equation (4). The resolution of the paradox is the substantial effect that stellar gas recycling has on the disk lifetimes.

6.2. *Recycling Model*

Most models of disk evolution treat stellar gas return in the instantaneous recycling approximation, i.e., a total return fraction is integrated over the entire IMF, and applied with no time delay. This approximation we applied in the analyses of gas consumption times by Larson et al. (1980) and Kennicutt (1983), using a return fraction $R = 0.20$ from Tinsley (1980). In retrospect, it is clear that this correction seriously underestimates the effect of recycling on the gas depletion times. Revisions to stellar evolution models and IMFs since 1980 significantly increase the integrated return fraction over Tinsley's estimate. In addition, the delayed return from low-mass stars can significantly lengthen the gas consumption timescale over that calculated using instantaneous recycling, as demonstrated for the Galactic disk by Ostriker & Thuan (1975). We now explore these effects by computing time-dependent disk evolution models with updated stellar input parameters.

We first calculated the time dependence of the mass return rate for a single-age stellar population. The necessary input parameters are the stellar initial versus final mass relation, the stellar lifetime versus mass relation, and the IMF. We adopted the initial-final mass relation of Weidemann (1987) for stars with initial masses of 1–8 $M_\odot$. Stars with these masses produce remnant masses of 0.55 to 1.55 $M_\odot$, resulting in 50%–81% of the initial mass being returned to the interstellar medium. Stars below 1 $M_\odot$ were assumed to be unevolving (assumed disk age 10 Gyr), while stars with $M_i = 8$–100 $M_\odot$ were assumed to return all but a 1.4 $M_\odot$ remnant (Arnett 1978). This ignores the possibility that very massive stars (>25 $M_\odot$) may produce black holes with much lower return fractions, but the total mass in this population is negligible for most realistic IMFs, so the distinction is unimportant for the application. Stellar lifetimes were taken from the solar composition models of Schaller et al. (1993). We calculated return rates for four IMFs, K83 ($\Gamma = -0.4$ for 0.1–1 $M_\odot$, -1.5 for 1–100 $M_\odot$), Salpeter, and the solar neighborhood IMFs of Scalo (1986) and Kroupa et al. (1993). Lower and upper mass limits of 0.1 and 100 $M_\odot$ were assumed in all cases. The return rates were integrated in time steps of 1 Gyr, except during the first Gyr when a time step of 200 Myr was used.

Figure 8 shows the time dependence of the integrated stellar return for the K83, S86, and Salpeter IMFs. The mass scale is normalized to the initial mass of the stellar population, so the plots show the fraction of the original mass returned in each 10^9 yr time step. In both cases and significant fraction of the gas is returned in the first 1 Gyr (over half in the first 200 Myr), followed by a slowly declining return rate over 1–10 Gyr. The Scalo IMF produces the least return at early times, but the most after 4 Gyr, due to the much steeper IMF slope above 1 $M_\odot$.

The total mass return fractions for all four IMFs are considerably higher than the 20% estimated by Tinsley (1980) and subsequently adopted by Larson et al. (1980) and K83. Over 10 Gyr the integrated return rates are 26%, 30%, 30%, and 46% for the S86, KTG93, Salpeter, and K83 IMFs, respectively. The return fraction listed for the S86 IMF is for the intermediate "best fit" IMF; the return fraction for the shallowest of the three Scalo (1986) IMFs is 47%. It is interesting to note that the total return fractions for the Salpeter and S86 IMFs are similar, even though the IMFs have radically different forms. This is because the relatively high return rate from massive stars in the Salpeter IMF is balanced by the large mass sink in unevolved stars below 1 $M_\odot$. Although the integrated return fractions are similar for the two IMF, Figure 8 shows that the respective time dependences for the return rates are markedly different.

To explore the effects on this return on disk evolution we then computed star formation histories for a grid of single-zone disk models. Disks were evolved by forming stars in 0.2–1

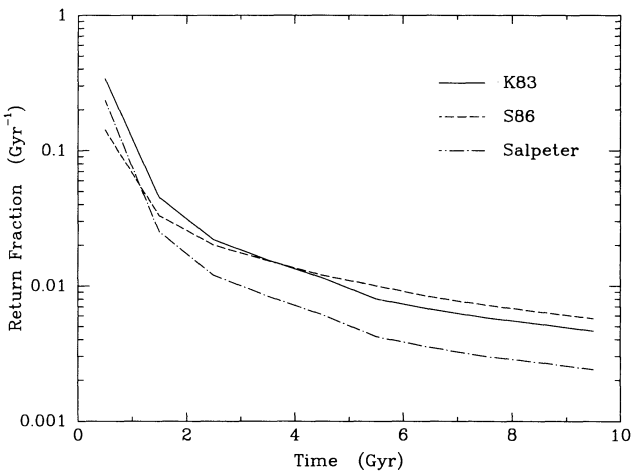

FIG. 8.—Time dependence of the stellar return rate for a single-age population. Rates are normalized to the total mass of the population. Most mass in the first time step (0–1 Gyr) is ejected in the first 200 Myr.

Gyr times steps, with star formation efficiencies ranging over 1%–50% per 10^8 yr. In most models the SFR was assumed to scale linearly with the available gas mass (linear Schmidt law), but a few additional models were calculated assuming a quadratic Schmidt law. At each time step the gas return each previous generation of stars was computed and added to the gas pool. Separate grids were run for mass return rates from a K83 and Scalo (1986) IMF. Final results were compared at a fixed disk age of 10 Gyr.

As an illustration of a typical model, Figure 9 shows the time evolution of the gas mass, stellar mass, SFR, and gas return rates for a disk with a K83 IMF and and star formation conversion efficiency of 4% of the gas mass per 10^8 yr. In this diagram all masses have been normalized to the total baryonic disk mass (gas plus stars). The SFR declines roughly linearly with time, as expected for the linear SFR versus gas density relation. After 10 Gyr the gas fraction in the disk has declined to 11%, and the mass of stars formed the last 1 Gyr is 5% of the disk mass; both parameters are typical of intermediate-type spirals (~Sb). However, close inspection of Figure 9 reveals that the gas return has affected the disk evolution in several important respects. Although stars now comprise 89% of the disk mass, the total mass of stars ever formed is actually 161% of the total mass; the 72% difference represents material which has been recycled. In this model gas is being returned at 62% of the rate at which it is being consumed by star formation. Hence even though the ratio of *current* gas mass to SFR implies a gas consumption time of only 2.5 Gyr, recycling is reducing the rate of gas depletion by a "recycling factor" $(1–0.62)^{-1} = 2.63$, so that the disk can actually sustain the current SFR for 6.6 Gyr.

The recycling factor is sensitive to several parameters, including the IMF (which determines the return fraction and its time dependence), and the star formation history, which is determined in the models by the star formation efficiency and the form of the SFR versus gas mass relation. Figure 10 shows the behavior of the recycling factor $(1 - \dot{M}/\mathrm{SFR})^{-1}$ for three sets of models, plotted versus disk gas fraction μ_{gas}. The solid lines show models with a K83 IMF, for a linear Schmidt law (lower line) and quadratic Schmidt law (upper line). The dashed line shows the results for a Scalo (S86) IMF with a linear Schmidt law. For slowly evolving disks with large present-day gas fractions the recycling correction approaches the asymptotic value $(1 - R)^{-1}$, where R is the bulk return fraction, 46% for the K83 IMF and 26% for the S86 IMF. The same recycling factor holds for disks with constant SFRs. However, for more rapidly evolving disks ($b \ll 1$ and $\mu_{\mathrm{gas}} \ll 1$) the recycling factor is much larger, because the delayed return from the more numerous old stars can approach or even exceed the present-day SFR.

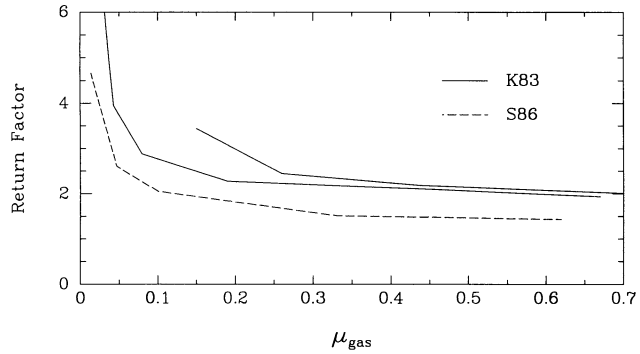

FIG. 10.—Correction factor to Roberts time from stellar recycling, for disk models with K83 IMF (*solid lines*) and S86 IMF (*dashed line*). Models are for a linear Schmidt star formation law, except for the upper curve, which assumes a quadratic Schmidt law.

Unfortunately the recycling correction cannot be determined a priori for any particular galaxy, because the correction is sensitive to the IMF and the temporal form of the past SFR. However, the models shown in Figure 10 should bracket the range of reasonable parameters. For values appropriate for most star forming disk galaxies ($\mu_{\mathrm{gas}} = 0.1–0.4$; $b = 0.1–1$) recycling extends the disk star formation by factors of 1.5–4. This means that star formation is likely to continue in most of the galaxies in Figure 7 for at least 4–10 Gyr. It is interesting to note that for gas-poor systems recycling is capable for sustain-

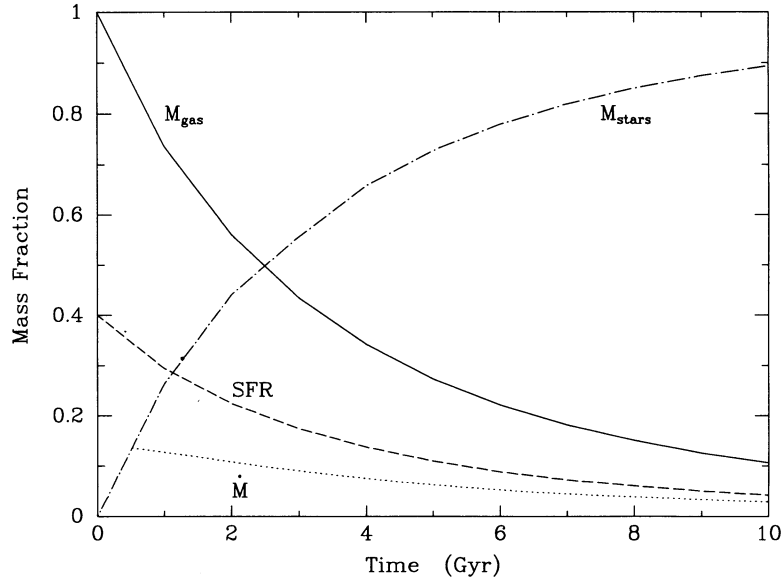

FIG. 9.—Time dependence of the gas mass, stellar mass, SFR, and gas return rate $\dot{M}$ for a disk model with K83 IMF and star formation efficiency of 4% per 10^8 yr. Units are disk mass fraction for gas and stellar masses, and disk mass fraction per Gyr for the SFR and $\dot{M}$.

ing star formation nearly indefinitely (Fig. 10), though at an absolute rate which is typically only a few percent or less of the mean past SFR.

These results may resolve the paradox of unrealistically short gas depletion times which was encountered by Larson et al. (1980) and Kennicutt (1983), and which is apparent in the distribution of uncorrected Roberts times in Figure 7. For typical recycling factors of 2–3 the star forming lifetime of *most* nearby disks is extended to values which are comparable to the Hubble time. It should be emphasized, however, that even when gas return is included, some of the galaxies in Figure 7 are expected to deplete their gas supplies at least to the level of the Jeans star formation threshold, within 2–3 Gyr. This should not be surprising. Figure 6 shows that the nearby universe contains numerous examples of spiral disks—the Sa–Sb galaxies—which today are forming stars at a small fraction of their past rate. It would indeed be surprising if some late-type, active disks were *not* being transformed to early-type systems at the present epoch.

7. SUMMARY

The main purpose of this paper has been to update the investigations of star formation histories of galaxies by Larson et al. (1980), Kennicutt (1983), and Gallagher et al. (1984), and to resolve some of the questions raised by those studies. As such it is useful to compare the conclusions of this analysis with the previous results.

1. We confirm the general picture presented initially by Roberts (1963), Searle et al. (1973), and Larson & Tinsley (1978), in which the observed differences in the photometric properties of S–Irr galaxies along the Hubble sequence are driven primary by a systematic change in the history of star formation. In the previous studies it was unclear whether these differences were primarily due to the gradient in disk/bulge fraction with Hubble type, or to changes in the stellar content and star formation histories of the disks. The results of this study clearly indicate that the changes in disk properties are the overwhelming contributor to the observed gradients in integrated properties of spirals. The SFR per unit stellar mass changes by orders of magnitude over the type range S0–Sd, while the disk fraction changes by factors of a few at most.

2. We find, in agreement with previous studies, that the photometric properties of S–Irr galaxies can be reproduced without invoking large variations in the stellar IMF. However, the observed photoionization rates in nearby spirals require an IMF which is enriched in massive stars by factors of at least 2–3 over the solar neighborhood IMFs of Miller & Scalo (1979) and Scalo (1986). We doubt that this discrepancy can be attributed to errors in the Hα observations or the photometric synthesis models. The discrepancy could be understood alternatively if the local samples of stars used to determine the Galactic IMF are deficient or incomplete) in massive stars, or if the IMF in active star forming regions is different from that in the solar neighborhood.

3. The excess of ionizing luminosity in disks, relative to that predicted for the solar neighborhood IMF, is in the same direction as the excess observed in infrared starburst galaxies (e.g., Rieke et al. 1993), but is less extreme. adopting the best fitting IMF from our observations of disk galaxies may relieve the need for lower mass IMF cutoffs in M82 and other infrared luminous starbursts.

4. When the current SFRs in disk galaxies are compared with the total available gas contents, the extrapolated Roberts times for gas consumption are of order ~ 3 Gyr on average, consistent with previous studies. However, a realistic time-dependent treatment of stellar recycling shows that recycling will extend the present SFRs by factors of 1.5–4 (or more), depending on the IMF and the past star formation history. For the range of IMFs considered here, the bulk return fraction from stars is 26%–46%, considerably higher than assumed in many previous studies. Consequently, the actual Roberts times for gas depletion in disks are of order 5–15 Gyr, sufficient to relative the need for disk accretion or infall to sustain star formation. However, some late-type galaxies show projected Roberts times of a few Gyr or less, even when recycling is included. These include galaxies undergoing short-lived star formation bursts, and other systems which will be transformed into early-type spirals in the near future.

5. The changes in disk SFRs per unit luminosity along the Hubble sequence appear to be much larger than the radial gradients in star formation history within individual disks. On the other hand, the changes in mean disk surface density along the Hubble sequence appear to be much smaller than the exponential gradients in surface density within disks. This combination of observations suggests that some parameter other than local gas surface density is the primary factor determining the timescale for star formation in galactic disks.

We are grateful to A. Maeder for transmitting the results of his stellar evolution models in advance of publication. We are also indebted to J. Ostriker and J. Gallagher for emphasizing to us the role of gas return in gas depletion calculations. A preliminary version of the recycling analysis was completed by C. W. C. as a Master's thesis at the University of Minnesota. This research was supported by the National Science Foundation through grant AST-9019150.

REFERENCES

Arnett, W. D. 1978, ApJ, 219, 1008
Bernlöhr, K. 1992, A&A, 263, 54
Bessell, M. 1979, PASP, 91, 589
Buat, V. 1992, A&A, 264, 444
Buat, V., Donas, J., & Deharveng, J. M. 1987, A&A, 185, 33
Byun, Y.-I. 1992, Ph.D. thesis, Australian National Univ.
Caldwell, N., Kennicutt, R., Phillips, A. C., & Schommer, R. A. 1991, ApJ, 370, 526
de Vaucouleurs, G., de Vaucouleurs, A., & Corwin, H. G. 1976, Second Reference Catalog of Bright Galaxies (Austin: Univ. Texas Press) (RC2)
de Vaucouleurs, G., de Vaucouleurs, A., Corwin, H. G., Jr. Buta, R. J., Paturel, G., & Fouqué, P. 1991, Third Reference Catalog of Bright Galaxies (New York: Springer Verlag) (RC3)
Devereux, N. A., & Young, J. S. 1991, ApJ, 371, 515
Donas, J., Deharveng, J. M., Laget, M., Milliard, B., & Huguenin, D. 1987, A&A, 180, 12
Faber, S. M., & Gallagher, J. S. 1979, ARA&A, 17, 135
Gallagher, J. S., Hunter, D. A., & Tutukov, A. V. 1984, ApJ, 284, 544
Green, E. M. 1988, in Calibration of Stellar Ages, ed. A. G. D. Philip (Schenectady: Davis), 81
Hummer, D. G., & Storey, P. J. 1987, MNRAS, 224, 801
Hunter, D. A., & Gallagher, J. S. 1985, ApJS, 58, 533
Israel, F. P., & Kennicutt, R. C. 1980, ApL, 21, 1
Israel, F. P., & van der Hulst, J. M. 1983, AJ, 88, 1736
Isserstedt, J., & Schindler, R. 1986, A&A, 167, 11
Joseph, R. 1991, in Massive Stars and Starbursts, ed. C. Leitherer, N. R. Walborn, T. M. Heckman, & C. A. Norman (Cambridge: Cambridge Univ. Press), 259
Kennicutt, R. C. 1983, ApJ, 272, 54 (K83)
———. 1986, in Stellar Populations, ed. C. Norman, A. Renzini, & M. Tosi (Cambridge: Cambridge Univ. Press), 125
———. 1989, ApJ, 344, 685
———. 1992, ApJ, 388, 310
———. 1993, in Mass-Transfer Induced Activity in Galaxies, ed. I. Shlosman (Cambridge: Cambridge Univ. Press), in press
Kennicutt, R. C., Edgar, B. K., & Hodge, P. W. 1989, ApJ, 337, 761

Kennicutt, R. C., Keel, W. C., van der Hulst, J. M., Hummel, E., & Roettiger, K. A. 1987, AJ, 93, 1011
Kennicutt, R. C., & Kent, S. M. 1983, AJ, 88, 1094
Kennicutt, R. C., & Martin, C. L. 1994, in preparation
Kent, S. M. 1986, AJ, 91, 1301
Koper, E., Dame, T. M., Israel, F. P., & Thaddeus, P. 1991, ApJ, 383, L11
Kroupa, P., Tout, C. A., & Gilmore, G. 1983, MNRAS, 262, 545 (KTG93)
Kurucz, R. L. 1992, private communication
Larson, R. B. 1986, MNRAS, 218, 409
———. 1992, in Star Fomation in Stellar Systems, ed. G. Tenorio-Tagle, M. Prieto, & F. Sánchez (Cambridge: Cambridge University Press), 125
Larson, R. B., & Tinsley, B. M. 1978, ApJ, 219, 46
Larson, R. B., Tinsley, B. M., & Caldwell, C. N. 1980, ApJ, 237, 692
Leitherer, C. 1990, ApJS, 73, 1
Maeder, A., & Meynet, G. 1989, A&A, 210, 155 (MM89)
Miller, G. E., & Scalo, J. M. 1979, ApJS, 41, 513
Oey, M. S., & Kennicutt, R. C. 1993, ApJ, 411, 137
Ostriker, J. P., & Thuan, T. X. 1975, ApJ, 202, 353
Parker, J. W., & Garmany, C. D. 1993, AJ, 106, 1471
Pfenniger, D., Combes, F., & Martinet, L. 1994, A&A, 285, 79
Pogge, R., & Eskridge, P. 1993, AJ, 106, 1405
Quark, W. J. 1972, ApJ, 176, L9
Rieke, G. H., Lebofsky, M. J., Thompson, R. I., Low, F. J., & Tokunaga, A. T. 1980, ApJ, 238, 24
Rieke, G. H., Loken, K., Rieke, M. J., & Tamblyn, P. 1993, ApJ, 412, 99
Roberts, M. S. 1963, ARAA, 1, 149
Roberts, M. S., & Haynes, M. P. 1994, ARAA, in press
Romanishin, W. 1990, AJ, 100, 373
Rubin, V. C. 1987, in Dark Matter in the Universe, ed. J. Kormendy & G. R. Knapp (Dordrecht: Reidel), 51
Ryder, S. D. 1993, Ph.D. thesis, Australian National Univ.
Sage, L. J. 1993, A&A, 272, 123
Salpeter, E. E. 1955, ApJ, 121, 161
Sandage, A. 1986, A&A, 161, 89
Sandage, A., & Tammann, G. A. 1981, A Revised Shapley-Ames Catalog of Bright Galaxies (Washington, DC: Carnegie Institution of Washington) (RSA)
Schaller, G., Schaerer, D., Meynet, G., & Maeder, A. 1993, A&AS, 96, 269 (SSMM93)
Scalo, J. M. 1986, Fund. Cos. Phys., 11, 1 (S86)
Searle, L., Sargent, W. L. W., & Bagnuolo, W. G. 1973, ApJ, 179, 427
Seidel, E., Demarque, P., & Weinberg, D. 1987, ApJS, 63, 917
Simien, F., & de Vaucouleurs, G. 1986, ApJ, 302, 564
Tinsley, B. M. 1980, Fund. Cos. Phys., 5, 287
Truran, J. W., & Cameron, A. G. W. 1971, Ap&SS, 14, 179
Vacca, W. D. 1994, ApJ, in press
van der Hulst, J. M., Kennicutt, R. C., Crane, P. C., & Rots, A. H. 1988, A&A, 195, 38
Walterbos, R. A. M., & Braun, R. 1994, ApJ, in press
Warmels, R. 1986, Ph.D. thesis, University of Groningen
Warmels, R. 1988, A&AS, 72, 427
Weidemann, V. 1987, A&A, 188, 74
White, S. D. M., & Frenk, C. S. 1991, ApJ, 379, 52
Young, J. S. 1990, in The Interstellar Medium in Galaxies, ed. H. A. Thronson, & J. M. Shull (Dordrecht: Kluwer), 67
Young, J. S., Xie, S., Kenney, J. D. P., & Rice, W. L. 1989, ApJS, 70, 699